GrowClust3D.jl: A Julia Package for the Relative Relocation of Earthquake Hypocenters Using 3D Velocity Models

Daniel T. Trugman[1], Calum J. Chamberlain[2], Alexandros Savvaidis[3], Anthony Lomax[4]

[1]Nevada Seismological Laboratory, University of Nevada, Reno, Reno NV, USA

[2]Victoria University of Wellington, Wellington, New Zealand

[3]Bureau of Economic Geology, Jackson School of Geosciences, The University of Texas at Austin, Austin TX, USA

[4]ALomax Scientific, Mouans-Sartoux, France

Corresponding author: Daniel Trugman (dtrugman@unr.edu)

Declaration of Competing Interests

The authors acknowledge there are no conflicts of interest recorded.

Abstract

Relative relocation techniques are widely used to improve the resolution of earthquake hypocenter positions. Here we present GrowClust3D.jl, an open-source software package written in the programming language Julia that builds and improves upon the original GrowClust algorithm, an established relative relocation technique based on cluster analysis instead of a more traditional matrix inversion approach. The adoption of Julia's modern programming environment allows for greater flexibility in GrowClust3D.jl's algorithm design and its computational implementation. Notable additions to the GrowClust3D.jl package include (i) several parallel processing options to improve efficiency in uncertainty quantification routines, (ii) incorporation of geographic map projections and station elevations during the relocation process, and (iii) the ability to use travel-time tables derived from 3D velocity models. We demonstrate the new features of the software package on relocation problems of different scales in Nevada, California, Texas, and New Zealand, where in the latter two cases the use of a 3D velocity model helps resolve structures that remain obscure with earlier versions of GrowClust. We expect that the new GrowClust3D.jl software package will become a valuable public resource for the earthquake science community.

Introduction

Catalogs of the location of earthquake hypocenters are one of the most fundamental derived-data products in seismology. Earthquake locations pervade nearly every aspect of earthquake science, from seismic monitoring, to tomographic imaging of Earth structure and fault networks, to detailed analyses of seismicity patterns, to development of fault-based hazard models (e.g., Ben-Menahem, 1995; Agnew, 2002). Because of this keystone role, one of the

primary missions of national and regional seismic monitoring networks is to provide public databases, or catalogs, of earthquake location estimates for events in their reporting region (e.g., Masse and Needham, 1989; Okada *et al.*, 2004; Hutton *et al.*, 2010; Guy *et al.*, 2015; Pankow *et al.*, 2019; Savvaidis *et al.*, 2019; Margheriti *et al.*, 2021). The basic methodology for determining these location estimates from seismic data is well-established (Buland, 1976). In a typical workflow, phase arrival times are marked by network analysts at a set of recording stations, and automated programs use a combination of grid search or linearized single-event inversion approaches (Geiger, 1912; Kennett and Engdahl, 1991; Klein, 2002) to determine the event location that best matches the observed phase arrivals with the timing predicted by travel time tables derived from a specific Earth model.

While this procedure seems straightforward at first glance, there are a number of complications in practice that create significant uncertainty and scatter in the reported location results (Bondár *et al.*, 2014; Karasözen and Karasözen, 2020). First, most earthquake location techniques rely on the capacity to accurately predict ray-based theoretical travel times from source to station. While this is a well-posed mathematical problem, it is made more challenging in practice due to our imperfect knowledge of subsurface structure. Lateral and depth-dependent variations in wavespeed that are not represented in these calculations will for example bias location estimates. Second, the precise timing of phase arrivals can be difficult to determine, especially for smaller earthquakes, waveforms with low signal-to-noise, or emergent phase arrivals. Third, inadequacy in the seismic monitoring network or station coverage can hinder location algorithms (Lomax and Savvaidis, 2019). These three forms of uncertainty – from the subsurface earth model, the determination of arrival times, and from the network geometry – routinely generate enough scatter in reported catalog locations to significantly hinder their utility

for scientific purposes, especially in cases with sparse network geometry (Lomax *et al.*, 2000; Myers *et al.*, 2007; Bondár and McLaughlin, 2009).

A well-tested solution to this dilemma is to refine the initial set of catalog locations using relative relocation algorithms (Got *et al.*, 1994). The basic idea behind these algorithms is to consider measurements of differential travel times from pairs of nearby earthquakes recorded at a set of common stations. This has the advantage of canceling out much of the effect of unmodeled subsurface structure on the ray-theoretical travel times, since the events are in close proximity and thus share much of the same raypath from source to station (Wolfe, 2002). In addition, if differential travel times are measured through waveform cross-correlation rather than by visual inspection, the measurement precision can be improved by more than an order of magnitude to the subsample level (Fremont and Malone, 1987). These concepts form the basis of publicly available "double-difference" software packages like HypoDD (Waldhauser and Ellsworth, 2000, 2002; Waldhauser and Schaff, 2008) and later GrowClust (Trugman & Shearer, 2017) that have become widely adopted by the seismology research community.

This article focuses on the GrowClust algorithm, which solves a differential form of the classic earthquake location problem using cluster analysis and graph theory instead of more traditional matrix inversion approaches. This formulation has several advantages, including numerical stability and efficient scaling to large-scale earthquake location problems with multiple seismicity clusters (Matoza *et al.*, 2013; Ross, Trugman, *et al.*, 2019; Skoumal *et al.*, 2019; Trugman *et al.*, 2020), and the ease of incorporating robust optimization routines during the relocation process to prevent measurement noise from compromising the results (Shearer, 1997). For these reasons, or perhaps others that are less quantifiable like reported ease-of-use and user-friendly documentation, GrowClust has become increasingly popular since its first public

release as a Fortran90 software package in 2017, with numerous applications at local and regional scales across the world (Chaves *et al.*, 2017; Trugman *et al.*, 2017; Hatch *et al.*, 2018; Koper *et al.*, 2018; Pang *et al.*, 2018; Rubinstein *et al.*, 2018; Pang *et al.*, 2019; Ross, Trugman, *et al.*, 2019; Shaddox and Schwartz, 2019; Skoumal *et al.*, 2019; Hatch *et al.*, 2020; Hauksson, Olson, *et al.*, 2020; Pang *et al.*, 2020; Ross *et al.*, 2020; Alongi *et al.*, 2021; Benson *et al.*, 2021; Chamberlain *et al.*, 2021; Glasgow *et al.*, 2021; Li *et al.*, 2021; Matoza *et al.*, 2021; Ross and Cochran, 2021; Beaucé *et al.*, 2022; Gong *et al.*, 2022; Hatch-Ibarra *et al.*, 2022; Okamoto *et al.*, 2022).

Current popularity notwithstanding, there is always room for improvement. This article describes a significant update and re-release of the original GrowClust algorithm in the programming language Julia, which has seen rapid growth in user base in the scientific computing community (Bezanson *et al.*, 2017). As we will demonstrate in the following sections, this choice brings about numerous advantages and opportunities for users of GrowClust3D.jl, including (i) automated parallelization of bootstrap resampling routines, rendering uncertainty quantification simple and efficient, (ii) embedding within the Julia ecosystem for easy import of powerful external packages, (iii) more efficient use of computer memory that removes the need for fixed array sizes, and perhaps most importantly, (iv) the ability to perform relocation problems in cases with 3D velocity models. This article is organized as follows: First, we briefly review the core GrowClust algorithm and philosophy (which remains largely unchanged) while highlighting differences with the new GrowClust3D.jl software. Next, we present a series of applications in different study regions to demonstrate the use of the software in various scenarios. Finally, we discuss the various advantages of adopting the new software package, while outlining current limitations and opportunities for future improvements.

Methods

Review of the GrowClust algorithm

Whether implemented in Fortran90 or Julia, the overarching goal of the program is to take a set of input locations from an earthquake catalog and refine the hypocentral positions (longitude, latitude, depth, and origin time) using observational constraints from waveform cross-correlation. GrowClust's tactic to achieve this goal is to treat the problem from a cluster analysis and graph-theoretical perspective. For each earthquake pair, the algorithm computes a waveform similarity coefficient in which higher values are meant to represent higher waveform similarity and thus more reliable differential time measurements. Using these coefficients, GrowClust undertakes agglomerative clustering (Kaufman and Rousseeuw, 2009; Frades and Matthiesen, 2010), where each event starts out as its own cluster of one and is progressively linked to other similar events in sequence, starting with the most similar event pair to ensure that earthquake pairs with high-quality differential time measurements are the foundation of the relocation set. Each time an event pair is linked, the events (and the clusters to which the event pairs belong) are relocated with respect to one another using a nested grid search approach designed to improve the match between the observed and ray-theoretical differential travel times. Event pair and cluster linkages are sometimes rejected if they violate user-specified quality control criteria. Because of this, when the relocation algorithm completes, there will still be a number of singleton events (clusters of one) that are not relocated and thus remain at their initial position.

GrowClust requires four main input datasets and an algorithm control file specifying things like filepaths and run parameters. The requisite datasets include (i) an earthquake catalog

specifying the initial locations of the event set to be relocated, (ii) a station list specifying the positions of the stations where differential time measurements are recorded, (iii) a cross-correlation file enumerating differential time measurements for pairs of events recorded at common stations, and (iv) a velocity model or alternative means to generate travel-time tables of theoretical arrival times. The control file organizes these input datasets, specifies the location of the output files to be generated, and gives the user some flexibility on the clustering hyperparameters and quality control criteria that suites their dataset. More details on these choices are provided in Trugman & Shearer (2017) and the online software documentation.

Key modifications of the GrowClust3D.jl algorithm

From a user perspective, the most obvious difference between this original implementation of GrowClust and GrowClust3D.jl is of course the driving programming language: Julia instead of Fortran90 in the original release. While this change may present an obstacle for some, the Julia user base is growing rapidly and the software features a diverse set of packages that can be applied to various problems in scientific computing (Bezanson *et al.*, 2017). Julia presents a user-friendly and flexible interface like Python, but if written carefully it can provide significant advantages in computational efficiency and can indeed be wall-clock competitive with compiled languages like C and Fortran (Bezanson *et al.*, 2017). We expect that users familiar with another programming language will be able to re-use or modify the examples presented in the online repository simply to suit their purposes.

The motivation behind the switch to Julia is to take advantage of several opportunities that comprise the bulk of the modifications in algorithm design (Figure 1). Perhaps the most notable new feature is much expanded flexibility in computing ray theoretical travel times. Just

like in the original implementation, GrowClust3D.jl can generate its own travel-time tables given an input 1D velocity model. The new implementation will generate a separate travel-time table for each station location that accounts for the listed station elevation, a detail that was neglected for the purposes of simplicity in the original Fortran90 codes. This approximation worked out in most (but not all) cases because station-specific effects on travel time will often cancel out in differential measurements. The more important new feature in GrowClust3D.jl is the capability to use travel-time tables generated from fully 3D velocity models, where wavespeeds vary both laterally and vertically. In the current version, this feature is implemented by reading in station-specific 3D travel time grids generated by NonLinLoc (Lomax *et al.*, 2000, 2009), which is an open-source program that can applied to the task of absolute earthquake location. This integration allows for the absolute and relative locations of output catalogs to be internally self-consistent, which mitigates the potential for unwanted biases or offsets in areas with complex velocity structures.

Another useful feature available in the Julia implementation is the ability to parallelize the bootstrap resampling routines used for uncertainty quantification. The original Fortran90 release implemented these routines in serial, so performing 100 bootstrap resamples required a runtime of ~100x relative to a runtime with no uncertainty quantification. In GrowClust3D.jl, resampling can be readily accomplished through either multithreading on a single computational core or multiprocessing on different cores. As we will demonstrate below, this parallelization can be a significant speed boost for large-scale problems, especially on computing servers with multiple cores.

There are several other minor differences worth discussion. While the original GrowClust software relied on simplified geographic transformations, GrowClust3D.jl wraps around the

PROJ cartographic library (PROJ contributors, 2022) with formal, user-selected map projections. One common complaint with the Fortran90 implementation is that it uses fixed array sizes for the differential time data, which caused compilation issues on machines with limited memory. The Julia implementation determines appropriate array sizes on the fly and is thus more user-friendly and memory efficient. The input file control parameters remain largely the same, with the exception of new specifications for travel time grid and map projection options. The core relocation algorithm and default hyperparameters are only slightly modified based on user feedback and algorithm performance on new datasets since the original publication. One important modification is that the GrowClust3D.jl software uses a different definition of waveform similarity to rank event pairs in the clustering algorithm. The new definition mitigates a potential issue the original algorithm had in penalizing highly similar event pairs that are recorded at fewer stations while elevating less similar but better-recorded event pairs.

Applications

We demonstrate the new software on different benchmark problems that highlight different features of the revised codes. Several of the datasets presented below have been studied in some capacity in other published works; it is our intention here to simply use them as case study examples of how GrowClust3D.jl can be applied as a scientific research tool.

Spanish Springs Sequence, Nevada

We begin with a reanalysis of the Spanish Springs earthquakes, a sequence of events occurring beneath the Reno suburb in 2012–2015. This spatially compact sequence included a M4.2 mainshock and more than a thousand smaller earthquakes detected by the Nevada Seismological Laboratory (NSL) and has become the canonical GrowClust example since its

194 inclusion the online tutorial with the initial software release (Trugman & Shearer, 2017). Here
195 we use the same input datasets to demonstrate that GrowClust3D.jl produces similar results as
196 the initial release when applied in a comparable way with the same 1D velocity model. To
197 quantify similarity, we measure the location offset between relocated hypocenters from the
198 original GrowClust software and GrowClust3D.jl. For relocated events, the median horizontal
199 and vertical offsets of 12.5 and 38.0 m are comparable to the relative location uncertainty
200 obtained through bootstrap resampling (11.0 and 51.0 m). The slight differences in location arise
201 due to fact that the ray-tracing algorithm in the GrowClust3D.jl explicitly accounts for variations
202 in station elevation (which is neglected in the original GrowClust) and the choice of map
203 projection in GrowClust3D.jl, another feature that is not an option in the original GrowClust.

204 Due in part to its proximity to Reno, the Spanish Springs sequence was well-recorded by
205 stations operated by the NSL and includes 1616 events reviewed by NSL analysts over the study
206 period. Many of the recorded events are quite small (< M1) and difficult to manually locate and
207 determine phase arrivals, which produces considerable scatter of the input catalog (Figure 2a).
208 Application of GrowClust3D.jl to this sequence significantly refines the hypocentral positions
209 (Figure 2b), revealing clear and vertically dipping fault structures. There is a section along the
210 mainshock fault plane that is relatively devoid of aftershock activity; this may be the section of
211 peak slip with stress concentrations around its periphery. The results presented here are quite
212 similar to those reported in the original GrowClust manuscript (Trugman & Shearer, 2017), and
213 are largely independent of new features employed (choice of map projection, ray tracing solver,
214 etc.). In all cases, the major structural features and pattern of relocated seismicity are visually

identical. The sequence thus remains a useful benchmark and can be used a simple test case for GrowClust users interesting in exploring the new software.

Ridgecrest Sequence, California

If the Spanish Springs sequence represents a useful, small-scale test case for GrowClust3D.jl, the July 2019 Ridgecrest sequence (e.g., Barnhart *et al.*, 2019; Ross, Idini, *et al.*, 2019; Lin, 2020; Lomax, 2020; Shelly, 2020) represents an opposite end-member case of a large-scale relocation problem with hundreds of discrete clusters and structural features to resolve over a ~100 km length scale. Here we apply GrowClust3D.jl to the input catalog and waveform cross-correlation dataset described in Trugman (2020) and Trugman *et al.* (2020) as a demonstration test case to gain insight and performance benchmarks of the new codes when applied on a large-scale relocation problem. We use the same local 1D velocity model as the original studies (Hauksson and Unruh, 2007) and GrowClust3D.jl's internal ray-tracing solver to generate the needed travel time tables, which are now station-specific to explicitly account for each station's elevation above mean sea level. Relocations are done using a Transverse Mercator map projection but otherwise use the same algorithm control parameters as the prior studies.

The GrowClust3D.jl relocations (Figure 3) are visually much more tightly constrained to clusters or linear features than the input catalog from the Southern California Earthquake Data Center. These locations highlight the remarkable structural complexity and fault architecture of the Ridgecrest sequence, which features hundreds of cross-cutting faults and branches off of the northwest-trending mainshock rupture plane (Liu *et al.*, 2019; Ross, Idini, *et al.*, 2019; Goldberg *et al.*, 2020; Lin, 2020; Lomax, 2020; Shelly, 2020). These structures, as well as the detailed relative depth-distribution of seismicity, are clearly better resolved in the relocated hypocenters

(Figure 4). Despite the challenging operational environment with high levels of noise that hinder traditional approaches to earthquake location (Hauksson, Yoon, *et al.*, 2020), the dense seismicity and high-quality cross-correlation measurements allow us to relocate the large majority (38278/43742 = 87.5%) of the events in the catalog.

Because of the large problem size, the Ridgecrest sequence also forms an instructive benchmark of the computational performance of the algorithm. Of particular interest here are the speedups in runtime observed when employing the new parallel processing tools in GrowClust3D.jl, which are designed to accelerate uncertainty quantification through parallelized bootstrap resampling. In the GrowClust3D Julia implementation, there are two distinct ways to do this: by multithreading – parallel computational threads on a single processor with shared memory, and multiprocessing – parallelization of multiple processors or computational cores without shared memory. This capability for non-expert users to readily incorporate parallel processing tools directly in their programs is a notable strength of the Julia language (Edelman, 2015; Besard *et al.*, 2019; Gao *et al.*, 2020) that GrowClust3D.jl leverages in its algorithm design.

Here we perform computational experiments on a mid-scale computing server with a 32-core, 64-thread chip (AMD EPYC-7532) where each computing core has a base 2.4 GHz clockspeed. In one set of experiments, we parallelize 100 bootstrap resampling runs using Julia's multithreading capabilities with different numbers of threads requested, tracking the total runtime of each experiment. In another, we perform an analogous set of experiments via (hyperthreaded) multiprocessing rather than multithreading on a single core. A comparison of these two experiments is presented in Figure 5. As expected, in multiprocessing mode there is a linear improvement in runtime with the number of cores employed. In multithreading mode,

runtime improvement is limited by computer memory and threading constraints, and thus saturates after threading resources are expended. While the precise saturation point depends on the platform and problem size, the basic concept does not. Multithreading provides a simple way of accelerating runtimes by a modest amount (2-4x), further gains require multiprocessing on discrete cores and scales linearly with the number of cores available.

Coyanosa, West Texas

By design, GrowClust3D.jl performs relative relocation, keeping the mean hypocentral position of earthquakes in each cluster fixed. Thus, while the method can be used to refine hypocentral positions, the absolute locations are intrinsically tied to the original input catalog. When using GrowClust3D.jl, it is therefore important to be as consistent as possible with the method used to obtain the original, absolute locations of the events of interest. The new software facilitates this consistency with its capability to directly read the travel time grids associated with 1D or 3D velocity models that are generated by NonLinLoc (Lomax et al., 2000, 2009), an open-source earthquake location and analysis package that can be used to constrain hypocentral positions and uncertainties from phase arrival data and an assumed velocity model.

Here we demonstrate the capability to use 3D travel time grids on a small test case in the Delaware Basin of West Texas, where seismicity rates have risen sharply in tandem with increased hydrocarbon production (e.g., Frohlich *et al.*, 2020; Savvaidis *et al.*, 2020; Skoumal *et al.*, 2020; Skoumal and Trugman, 2021; Trugman and Savvaidis, 2021). Our study region for this exercise centers on clusters of seismicity near Coyanosa, Texas in the southern portion of the Basin. We begin with an event set of 901 earthquakes occurring from January 2017 through May 2022, taken from the TexNet earthquake catalog (https://catalog.texnet.beg.utexas.edu/), which

assumes a regional 1D velocity model. We then attempt to relocate all earthquakes in this dataset which have 4 or more arrivals using NonLinLoc, assuming an Azimuthal Equidistant projection (an appropriate choice in that the projection aims to accurately preserve distances from the center of the study region) and using a 3D velocity model derived from local geologic, active seismic, and well-based constraints. A subset of the initial NonLinLoc solutions are not viable, with depths that are artificially pinned to the surface. This artifact can occur for small events with limited and poorly resolved phase arrivals, combined ray path and travel-time complexity due to a shallow, high-velocity evaporite layer characteristic of the Permian Basin (Savvaidis *et al.*, 2022). To avoid compromising our final depth estimates, we remove these outlier events from our analysis and further refine the position of the remaining, 794, quality-controlled events using available differential travel time measurements and GrowClust3D.jl, assuming the same velocity model and projection, resulting in a final relocated catalog contains 364 events.

The results of this analysis workflow are presented in Figure 6. In this case, use of a location-specific 3D velocity model improves the lateral and depth resolution of the absolute locations, which are noticeably shallower than the initial TexNet catalog, in line with other recent findings (Savvaidis *et al.*, 2021; Sheng *et al.*, 2022). GrowClust3D.jl builds on this improvement by further resolving the relative positions, revealing hidden linear features which correspond to known, northwest-trending shallow normal faults and graben structures in the Delaware Basin (Staniewicz *et al.*, 2020; Hennings *et al.*, 2021; Horne *et al.*, 2021). The GrowClust3D.jl depth distribution is concentrated in the 0–3.5 km range and peaks near 2 km depth, perhaps a signature of triggering from anthropogenic stressing. The improved resolution of hypocentral depths provided by techniques like GrowClust3D.jl may be key to understanding causal factors

driving seismicity in this region (Savvaidis *et al.*, 2020; Skoumal *et al.*, 2020; Zhai *et al.*, 2021; Sheng *et al.*, 2022).

Kaikōura Aftershocks, New Zealand

The most notable new feature of the software is the capability to perform relocation tasks that require 3D velocity models with strong lateral variations in Earth structure. This need is perhaps most pronounced in subduction zone settings, where the dipping interface of the subducting slab and overriding plate creates a baseline geometric feature upon which additional structural complexity is nearly always present. Here we consider a relocation problem of the earthquakes surrounding the rupture of the 2016 M7.8 Kaikōura, New Zealand earthquake, which triggered tens of thousands of aftershocks dominantly on crustal faults above the Hikurangi Subduction Zone (Holden *et al.*, 2017; Ulrich *et al.*, 2019; Chamberlain *et al.*, 2021). Perhaps even more so than Ridgecrest, the Kaikōura rupture is remarkable for its complexity, stitching together at least 21 faults across the South Island of New Zealand (Cesca *et al.*, 2017; Hamling *et al.*, 2017; Holden *et al.*, 2017; Kaiser *et al.*, 2017; Zhang *et al.*, 2017) and potentially involving rupture of the underlying subduction interface (e.g., Mouslopoulou *et al.*, 2019).

Chamberlain et al. (2021) performed a template-matching exercise to detect small earthquakes and applied the original GrowClust algorithm with a 1D cross-section of the 3D tomographic model of Eberhart-Phillips and Bannister (2015). Due to the limitations of the original template-matching catalog, especially the sparse station coverage and limitations in the relocation technique (which assumed a single 1D velocity model for the entire study region), resolution of the sequence could certainly be improved. Here we build on the results of Chamberlain (2021) by using the same input catalog and differential time measurements, but

now taking advantage of the new capabilities of the GrowClust3D.jl software to directly use travel time grids derived from a 3D earth model – NZ3D version 2.2 (Eberhart-Phillips and Bannister, 2015; Henrys *et al.*, 2020) – during the relocation process. The input, absolute locations are the same in both cases and were obtained with NonLinLoc (Lomax *et al.*, 2000, 2009). Relocations are performed in a Transverse Mercator projection rotated 140 degrees along the strike of the New Zealand islands, following Eberhart-Phillips and Bannister (2015).

Relocation results for the Kaikōura sequence are summarized in Figure 7, with select cross-section comparisons to original GrowClust results of Chamberlain et al. (2021) in Figure 8. Most of the detected aftershocks are crustal events, well above the Hikurangi megathrust interface depth determined by Williams *et al.* (2013). Very few events appear to locate on the interface itself. Comparing the original and new relocations, we observe a notable sharpening in the seismicity in certain areas, likely in relation to the strength of the lateral variations in wavespeed. For example, the activation of splay faults above the megathrust interface can be seen in cross-sections C and D (Figure 8) using the GrowClust3D.jl locations, but these structural features are not readily visible in identical cross-sections from the original 1D relocation results. These promising results for Kaikōura suggest promise for future applications of the new software in subduction zone settings, even when station coverage is limited (Figure 7).

Outlook and Future Directions

In this article we present GrowClust3D.jl, a significant advancement over the original GrowClust software for the relative relocation of earthquake hypocenters. Now rewritten in the programming language Julia, the open-source software package follows the same conceptual

paradigm of the original release but contains a number of new features and options we hope will prove useful to the scientific community. The most notable of these is the capability to use 3D velocity models and travel time grids produced by NonLinLoc, ensuring the absolute and relative hypocenters are self-consistent and allowing for improved precision in regions with strong lateral heterogeneity in wavespeed. The new relocation codes also make it simple to parallelize bootstrap uncertainty quantification using multithreading or multiprocessing, resulting in improvements in speed of a factor of 20 or more on large-scale problems, depending on available resources. The new Julia implementation can also make more efficient use of available computer memory because it does not require the user to compile fixed array sizes prior to runtime. Other minor improvements include the incorporation of standardized map projection routines and the explicit accounting of station elevations, factors that were neglected in the original release of the program.

Having GrowClust3D as part of the broader Julia ecosystem makes it easier to update the package based on user feedback while opening up new opportunities for additional user flexibility and creativity. The codes already leverage widely used Julia packages, notably ones for statistical and array calculations, interpolations, map projections, and tabular datasets. The codes are deliberately modular in design, which makes it simple for users to modify short sections of codes to suit their scientific objectives. A good example of this is the metric used to define event pair similarity. In the original Fortran implementation of GrowClust, this was a simple summation of cross-correlation coefficients across all stations recording an event pair. This definition, while functional and straightforward, had the tendency to overweight event pairs with more cross-correlation measurements at the expense of highly similar pairs with fewer recordings. The new Julia implementation modifies this definition by considering only a fixed

number of stations for all event pairs, the specifics of which can be modified by the user. In Julia, one could easily implement customized metrics to achieve different goals, for example by differentiating template matching pairs from pairs of analyst-reviewed events.

The current implementation of GrowClust3D.jl described here has several limitations to be aware of, some of which could be addressed in future releases pending user interest and feedback. In the current version, GrowClust3D.jl can perform simple 1D ray tracing tasks but does not include a full eikonal equation solver for 3D problems, instead relying on external programs like NonLinLoc to facilitate these calculations. This approach has the advantage of consistency with the input catalog and removes the computationally expensive step of 3D ray tracing but does limit user capabilities for certain problems. Future implementations could feature an internal eikonal equation solver or integrate with other location packages beyond NonLinLoc. Note, GrowClust3D.jl itself only performs relative relocation and not the initial, absolute location. This choice is deliberate because it allows the user to select their own suitable method based on their data and preferences, but it does limit the software in some ways. Likewise, the software requires the user to pre-compute differential travel times from waveform cross-correlation, using any technique they deem sufficient. It may be possible in future to integrate with Julia waveform processing tools like SeisIO (Jones *et al.*, 2020) to help facilitate this step more directly. In addition, relocation packages like HypoDD (Waldhauser and Ellsworth, 2000) have long used catalog differential times in complement to those derived from waveform cross-correlation. This option could be considered if warranted from a value-added standpoint. There are many more possibilities consider; the beauty of an open-source tool like

GrowClust3D.jl is that the potential for improvement is bounded only by user imagination and energy.

Data and Resources

The software described in this study is documented and publicly available in the repository: https://github.com/dttrugman/GrowClust3D. The original GrowClust software is still available at: https://github.com/dttrugman/GrowClust. We thank developers of Julia (Bezanson *et al.*, 2017), NonLinLoc (Lomax *et al.*, 2000), PROJ (PROJ contributors, 2022), and the Generic Mapping Toolbox (Wessel *et al.*, 2019) for publicly available software tools used in the implementation and presentation of this study. Earthquake catalog and waveform data from the Nevada Seismological Laboratory (http://www.seismo.unr.edu/), Southern California Earthquake Data Center (https://scedc.caltech.edu/index.html), TexNet (https://www.beg.utexas.edu/texnet-cisr/texnet), and GeoNet (https://www.geonet.org.nz/) were used to derive inputs for the relocation algorithm. The 3D compressional wave model and its travel time grids (assuming a constant Vp/Vs of 1.7) for the Coyanosa case study are available on the Texas Data Repository (https://doi.org/10.18738/T8/RQGQ9D), where we have made the relocated catalogs produced in this study publicly available (https://doi.org/10.18738/T8/44T2X8). The 3D velocity model used for the New Zealand case study are archived on Zenodo (https://zenodo.org/record/3779523#.YzsAi-zMJoM).

Acknowledgments

The authors have no real or perceived financial or conflicts of interest related to the publication of this study. D. Trugman gratefully acknowledges support from NSF Award EAR-2121666 and the State of Texas through TexNet (Seismic Monitoring and Seismicity Research Project). A.

Savvaidis and A. Lomax grateful acknowledge support from the State of Texas through TexNet (Seismic Monitoring and Seismicity Research Project). C. Chamberlain is grateful to the New Zealand Ministry of Business, Innovation and Employment for funding through the Endeavour Programme: "Rapid Characterization of Earthquakes and Tsunamis (RCET)". Scientific discussions with Steve Grand, Thorsten Becker, Laura Wallace were valuable in guiding this project. We thank the Associate Editor and constructive peer reviews from R. Wang and R. Skoumal for suggestions that substantively improved the manuscript.

References

Agnew, D. C. (2002). History of seismology, in *International Handbook of Earthquake and Engineering Seismology*, Elsevier, 3–11, doi: 10.1016/S0074-6142(02)80203-0.

Alongi, T., S. Y. Schwartz, H. R. Shaddox, and D. T. Small (2021). Probing the Southern Cascadia Plate Interface With the Dense Amphibious Cascadia Initiative Seismic Array, *Journal of Geophysical Research: Solid Earth* **126**, no. 7, e2021JB022180, doi: 10.1029/2021JB022180.

Barnhart, W. D., G. P. Hayes, and R. D. Gold (2019). The July 2019 Ridgecrest, California, Earthquake Sequence: Kinematics of Slip and Stressing in Cross-Fault Ruptures, *Geophysical Research Letters* **46**, no. 21, 11859–11867, doi: 10.1029/2019GL084741.

Beaucé, E., R. D. van der Hilst, and M. Campillo (2022). Microseismic Constraints on the Mechanical State of the North Anatolian Fault Zone 13 Years After the 1999 M7.4 Izmit Earthquake, *Journal of Geophysical Research: Solid Earth* **127**, no. 9, e2022JB024416, doi: 10.1029/2022JB024416.

Ben-Menahem, A. (1995). A concise history of mainstream seismology: Origins, legacy, and perspectives, *Bulletin of the Seismological Society of America* **85**, no. 4, 1202–1225.

Benson, T. W., F. Illsley-Kemp, H. C. Elms, I. J. Hamling, M. K. Savage, C. J. N. Wilson, E. R. H. Mestel, and S. J. Barker (2021). Earthquake Analysis Suggests Dyke Intrusion in 2019 Near Tarawera Volcano, New Zealand, *Frontiers in Earth Science* **8**.

Besard, T., C. Foket, and B. De Sutter (2019). Effective Extensible Programming: Unleashing Julia on GPUs, *IEEE Transactions on Parallel and Distributed Systems* **30**, no. 4, 827–841, doi: 10.1109/TPDS.2018.2872064.

Bezanson, J., A. Edelman, S. Karpinski, and V. B. Shah (2017). Julia: A fresh approach to numerical computing, *SIAM Review* **59**, no. 1, 65–98, doi: 10.1137/141000671.

Bondár, I., and K. McLaughlin (2009). Seismic location bias and uncertainty in the presence of correlated and non-Gaussian travel-time errors, *Bulletin of the Seismological Society of America* **99**, no. 1, 172–193.

Bondár, I., S. Myers, and E. R. Engdahl (2014). Earthquake location, in M. Beer, I. A. Kougioumtzoglou, E. Patelli, and I. Siu-Kui Au(Editors), Springer Verlag, Berlin, 1–18.

Buland, R. (1976). The mechanics of locating earthquakes, *Bulletin of the Seismological Society of America* **66**, no. 1, 173–187, doi: 10.1785/BSSA0660010173.

Cesca, S., Y. Zhang, V. Mouslopoulou, R. Wang, J. Saul, M. Savage, S. Heimann, S.-K. Kufner, O. Oncken, and T. Dahm (2017). Complex rupture process of the Mw 7.8, 2016, Kaikoura earthquake, New Zealand, and its aftershock sequence, *Earth and Planetary Science Letters* **478**, 110–120, doi: 10.1016/j.epsl.2017.08.024.

Chamberlain, C. J., W. B. Frank, F. Lanza, J. Townend, and E. Warren-Smith (2021). Illuminating the Pre-, Co-, and Post-Seismic Phases of the 2016 M7.8 Kaikōura Earthquake With 10 Years of Seismicity, *Journal of Geophysical Research: Solid Earth* **126**, no. 8, e2021JB022304, doi: 10.1029/2021JB022304.

Chaves, E. J., L. Duboeuf, S. Y. Schwartz, T. Lay, and J. Kintner (2017). Aftershocks of the 2012 Mw 7.6 Nicoya, Costa Rica, Earthquake and Mechanics of the Plate Interface, *Bulletin of the Seismological Society of America* **107**, no. 3, 1227–1239, doi: 10.1785/0120160283.

Eberhart-Phillips, D., and S. Bannister (2015). 3-D imaging of the northern Hikurangi subduction zone, New Zealand: variations in subducted sediment, slab fluids and slow slip, *Geophysical Journal International* **201**, no. 2, 838–855, doi: 10.1093/gji/ggv057.

Edelman, A. (2015). Julia: A fresh approach to parallel programming, in *2015 IEEE International Parallel and Distributed Processing Symposium*, 517–517, doi: 10.1109/IPDPS.2015.122.

Frades, I., and R. Matthiesen (2010). Overview on Techniques in Cluster Analysis, in *Bioinformatics Methods in Clinical Research* R. Matthiesen(Editor), Humana Press, Totowa, NJ, Methods in Molecular Biology, 81–107, doi: 10.1007/978-1-60327-194-3_5.

Fremont, M.-J., and S. D. Malone (1987). High precision relative locations of earthquakes at Mount St. Helens, Washington, *J. Geophys. Res.* **92**, no. B10, 10223–10236, doi: 10.1029/JB092iB10p10223.

Frohlich, C., C. Hayward, J. Rosenblit, C. Aiken, P. Hennings, A. Savvaidis, C. Lemons, E. Horne, J. I. Walter, and H. R. DeShon (2020). Onset and Cause of Increased Seismic Activity Near Pecos, West Texas, United States, From Observations at the Lajitas TXAR Seismic Array, *Journal of Geophysical Research: Solid Earth* **125**, no. 1, e2019JB017737, doi: 10.1029/2019JB017737.

Gao, K., G. Mei, F. Piccialli, S. Cuomo, J. Tu, and Z. Huo (2020). Julia language in machine learning: Algorithms, applications, and open issues, *Computer Science Review* **37**, 100254, doi: 10.1016/j.cosrev.2020.100254.

Geiger, L. (1912). Probability method for the determination of earthquake epicenters from the arrival time only, *Bull. St. Louis Univ* **8**, 60–71.

Glasgow, M., B. Schmandt, R. Wang, M. Zhang, S. L. Bilek, and E. Kiser (2021). Raton Basin Induced Seismicity Is Hosted by Networks of Short Basement Faults and Mimics Tectonic Earthquake Statistics, *Journal of Geophysical Research: Solid Earth* **126**, no. 11, e2021JB022839, doi: 10.1029/2021JB022839.

Goldberg, D. E., D. Melgar, V. J. Sahakian, A. M. Thomas, X. Xu, B. W. Crowell, and J. Geng (2020). Complex Rupture of an Immature Fault Zone: A Simultaneous Kinematic Model of the 2019 Ridgecrest, CA Earthquakes, *Geophysical Research Letters* **47**, no. 3, e2019GL086382, doi: 10.1029/2019GL086382.

Gong, J., W. Fan, and R. Parnell-Turner (2022). Microseismicity Indicates Atypical Small-Scale Plate Rotation at the Quebrada Transform Fault System, East Pacific Rise, *Geophysical Research Letters* **49**, no. 3, e2021GL097000, doi: 10.1029/2021GL097000.

Got, J.-L., J. Fréchet, and F. W. Klein (1994). Deep fault plane geometry inferred from multiplet relative relocation beneath the south flank of Kilauea, *J. Geophys. Res.* **99**, no. B8, 15375–15386, doi: 10.1029/94JB00577.

Guy, M. R., J. M. Patton, J. Fee, M. Hearne, E. Martinez, D. Ketchum, C. Worden, V. Quitoriano, E. Hunter, G. Smoczyk, *et al.* (2015). National Earthquake Information Center systems overview and integration, USGS Numbered Series 2015–1120, U.S. Geological Survey, Reston, VA, Open-File Report, 28 p., doi: 10.3133/ofr20151120.

Hamling, I. J., S. Hreinsdóttir, K. Clark, J. Elliott, C. Liang, E. Fielding, N. Litchfield, P. Villamor, L. Wallace, T. J. Wright, *et al.* (2017). Complex multifault rupture during the 2016 Mw 7.8 Kaikōura earthquake, New Zealand, *Science* **356**, no. 6334, eaam7194, doi: 10.1126/science.aam7194.

Hatch, R. L., R. E. Abercrombie, C. J. Ruhl, and K. D. Smith (2018). Earthquake Interaction, Fault Structure, and Source Properties of a Small Sequence in 2017 near Truckee, California, *Bulletin of the Seismological Society of America* **108**, no. 5A, 2580–2593, doi: 10.1785/0120180089.

Hatch, R. L., R. E. Abercrombie, C. J. Ruhl, and K. D. Smith (2020). Evidence of Aseismic and Fluid-Driven Processes in a Small Complex Seismic Swarm Near Virginia City, Nevada, *Geophysical Research Letters* **47**, no. 4, e2019GL085477, doi: 10.1029/2019GL085477.

Hatch-Ibarra, R. L., R. E. Abercrombie, C. J. Ruhl, K. D. Smith, W. C. Hammond, and I. K. Pierce (2022). The 2016 Nine Mile Ranch Earthquakes: Hazard and Tectonic Implications of Orthogonal Conjugate Faulting in the Walker Lane, *Bulletin of the Seismological Society of America* **112**, no. 3, 1727–1741, doi: 10.1785/0120210149.

Hauksson, E., B. Olson, A. Grant, J. R. Andrews, A. I. Chung, S. E. Hough, H. Kanamori, S. K. McBride, A. J. Michael, M. Page, *et al.* (2020). The Normal-Faulting 2020 Mw 5.8 Lone Pine, Eastern California, Earthquake Sequence, *Seismological Research Letters* **92**, no. 2A, 679–698, doi: 10.1785/0220200324.

Hauksson, E., and J. Unruh (2007). Regional tectonics of the Coso geothermal area along the intracontinental plate boundary in central eastern California: Three-dimensional Vp and Vp/Vs models, spatial-temporal seismicity patterns, and seismogenic deformation, *Journal of Geophysical Research: Solid Earth* **112**, no. B6, doi: 10.1029/2006JB004721.

Hauksson, E., C. Yoon, E. Yu, J. R. Andrews, M. Alvarez, R. Bhadha, and V. Thomas (2020). Caltech/USGS Southern California Seismic Network (SCSN) and Southern California Earthquake Data Center (SCEDC): Data Availability for the 2019 Ridgecrest Sequence, *Seismological Research Letters* **91**, no. 4, 1961–1970, doi: 10.1785/0220190290.

Hennings, P., N. Dvory, E. Horne, P. Li, A. Savvaidis, and M. Zoback (2021). Stability of the Fault Systems That Host-Induced Earthquakes in the Delaware Basin of West Texas and Southeast New Mexico, *The Seismic Record* **1**, no. 2, 96–106, doi: 10.1785/0320210020.

Henrys, S., D. Eberhart-Phillips, D. Bassett, R. Sutherland, D. Okaya, M. Savage, D. Evanzia, T. Stern, H. Sato, K. Mochizuki, *et al.* (2020). Upper Plate Heterogeneity Along the Southern Hikurangi Margin, New Zealand, *Geophysical Research Letters* **47**, no. 4, e2019GL085511, doi: 10.1029/2019GL085511.

Holden, C., Y. Kaneko, E. D'Anastasio, R. Benites, B. Fry, and I. J. Hamling (2017). The 2016 Kaikōura Earthquake Revealed by Kinematic Source Inversion and Seismic Wavefield Simulations: Slow Rupture Propagation on a Geometrically Complex Crustal Fault Network, *Geophysical Research Letters* **44**, no. 22, 11,320-11,328, doi: 10.1002/2017GL075301.

Horne, E. A., P. H. Hennings, and C. K. Zahm (2021). Basement-rooted faults of the Delaware Basin and Central Basin Platform, Permian Basin, West Texas and southeastern New Mexico, in *The Geologic Basement of Texas: A Volume in Honor of Peter T. Flawn; edited by O. A. Callahan and P. Eichhubl*, The University of Texas at Austin, Austin, TX, Bureau of Economic Geology Report of Investigations 286.

Hutton, K., J. Woessner, and E. Hauksson (2010). Earthquake Monitoring in Southern California for Seventy-Seven Years (1932-2008), *Bulletin of the Seismological Society of America* **100**, no. 2, 423–446, doi: 10.1785/0120090130.

Jones, J. P., K. Okubo, T. Clements, and M. A. Denolle (2020). SeisIO: A Fast, Efficient Geophysical Data Architecture for the Julia Language, *Seismological Research Letters* **91**, no. 4, 2368–2377, doi: 10.1785/0220190295.

Kaiser, A., N. Balfour, B. Fry, C. Holden, N. Litchfield, M. Gerstenberger, E. D'Anastasio, N. Horspool, G. McVerry, J. Ristau, *et al.* (2017). The 2016 Kaikōura, New Zealand, Earthquake: Preliminary Seismological Report, *Seismological Research Letters* **88**, no. 3, 727–739, doi: 10.1785/0220170018.

Karasözen, E., and B. Karasözen (2020). Earthquake location methods, *Int J Geomath* **11**, no. 1, 13, doi: 10.1007/s13137-020-00149-9.

Kaufman, L., and P. J. Rousseeuw (2009). *Finding Groups in Data: An Introduction to Cluster Analysis*, John Wiley & Sons.

Kennett, B. L. N., and E. R. Engdahl (1991). Traveltimes for global earthquake location and phase identification, *Geophysical Journal International* **105**, no. 2, 429–465, doi: 10.1111/j.1365-246X.1991.tb06724.x.

Klein, F. W. (2002). User's guide to HYPOINVERSE-2000, a Fortran program to solve for earthquake locations and magnitudes, Report 2002–171, U.S Dept. of the Interior, Geological Survey, Reston, VA, Open-File Report, 123 p.

Koper, K. D., K. L. Pankow, J. C. Pechmann, J. M. Hale, R. Burlacu, W. L. Yeck, H. M. Benz, R. B. Herrmann, D. T. Trugman, and P. M. Shearer (2018). Afterslip Enhanced Aftershock Activity During the 2017 Earthquake Sequence Near Sulphur Peak, Idaho, *Geophysical Research Letters* **45**, no. 11, 5352–5361, doi: 10.1029/2018GL078196.

Li, B. Q., J. D. Smith, and Z. E. Ross (2021). Basal nucleation and the prevalence of ascending swarms in Long Valley caldera, *Science Advances* **7**, no. 35, eabi8368, doi: 10.1126/sciadv.abi8368.

Lin, G. (2020). Waveform Cross-Correlation Relocation and Focal Mechanisms for the 2019 Ridgecrest Earthquake Sequence, *Seismological Research Letters* **91**, no. 4, 2055–2061, doi: 10.1785/0220190277.

Liu, C., T. Lay, E. E. Brodsky, K. Dascher-Cousineau, and X. Xiong (2019). Coseismic Rupture Process of the Large 2019 Ridgecrest Earthquakes From Joint Inversion of Geodetic and Seismological Observations, *Geophysical Research Letters* **46**, no. 21, 11820–11829, doi: 10.1029/2019GL084949.

Lomax, A. (2020). Absolute Location of 2019 Ridgecrest Seismicity Reveals a Shallow Mw 7.1 Hypocenter, Migrating and Pulsing Mw 7.1 Foreshocks, and Duplex Mw 6.4 Ruptures, *Bulletin of the Seismological Society of America* **110**, no. 4, 1845–1858, doi: 10.1785/0120200006.

Lomax, A., A. Michelini, and A. Curtis (2009). Earthquake Location, Direct, Global-Search Methods, in *Encyclopedia of Complexity and Systems Science* R. A. Meyers(Editor), Springer, New York, NY, 1–33, doi: 10.1007/978-3-642-27737-5_150-2.

Lomax, A., and A. Savvaidis (2019). Improving Absolute Earthquake Location in West Texas Using Probabilistic, Proxy Ground-Truth Station Corrections, *Journal of Geophysical Research: Solid Earth* **124**, no. 11, 11447–11465, doi: 10.1029/2019JB017727.

Lomax, A., J. Virieux, P. Volant, and C. Berge-Thierry (2000). Probabilistic Earthquake Location in 3D and Layered Models, in *Advances in Seismic Event Location* C. H. Thurber, and N. Rabinowitz(Editors),

Springer Netherlands, Dordrecht, Modern Approaches in Geophysics, 101–134, doi: 10.1007/978-94-015-9536-0_5.

Margheriti, L., C. Nostro, O. Cocina, M. Castellano, M. Moretti, V. Lauciani, M. Quintiliani, A. Bono, F. M. Mele, S. Pintore, *et al.* (2021). Seismic Surveillance and Earthquake Monitoring in Italy, *Seismological Research Letters*, doi: 10.1785/0220200380.

Masse, R. P., and R. E. Needham (1989). NEIC - the National Earthquake Information Center, *Earthquakes & Volcanoes (USGS)* **21**, no. 1, 4–44.

Matoza, R. S., P. G. Okubo, and P. M. Shearer (2021). Comprehensive High-Precision Relocation of Seismicity on the Island of Hawai‘i 1986–2018, *Earth Space Sci* **8**, no. 1, doi: 10.1029/2020EA001253.

Matoza, R. S., P. M. Shearer, G. Lin, C. J. Wolfe, and P. G. Okubo (2013). Systematic relocation of seismicity on Hawaii Island from 1992 to 2009 using waveform cross correlation and cluster analysis, *Journal of Geophysical Research: Solid Earth* **118**, no. 5, 2275–2288, doi: 10.1002/jgrb.50189.

Mouslopoulou, V., V. Saltogianni, A. Nicol, O. Oncken, J. Begg, A. Babeyko, S. Cesca, and M. Moreno (2019). Breaking a subduction-termination from top to bottom: The large 2016 Kaikōura Earthquake, New Zealand, *Earth and Planetary Science Letters* **506**, 221–230, doi: 10.1016/j.epsl.2018.10.020.

Myers, S. C., G. Johannesson, and W. Hanley (2007). A Bayesian hierarchical method for multiple-event seismic location, *Geophysical Journal International* **171**, no. 3, 1049–1063, doi: 10.1111/j.1365-246X.2007.03555.x.

Okada, Y., K. Kasahara, S. Hori, K. Obara, S. Sekiguchi, H. Fujiwara, and A. Yamamoto (2004). Recent progress of seismic observation networks in Japan —Hi-net, F-net, K-NET and KiK-net—, *Earth, Planets and Space* **56**, no. 8, xv–xxviii, doi: 10.1186/BF03353076.

Okamoto, K. K., H. M. Savage, E. S. Cochran, and K. M. Keranen (2022). Stress Heterogeneity as a Driver of Aseismic Slip During the 2011 Prague, Oklahoma Aftershock Sequence, *Journal of Geophysical Research: Solid Earth* **127**, no. 8, e2022JB024431, doi: 10.1029/2022JB024431.

Pang, G., K. D. Koper, J. M. Hale, R. Burlacu, J. Farrell, and R. B. Smith (2019). The 2017–2018 Maple Creek Earthquake Sequence in Yellowstone National Park, USA, *Geophysical Research Letters* **46**, no. 9, 4653–4663, doi: 10.1029/2019GL082376.

Pang, G., K. D. Koper, M. Mesimeri, K. L. Pankow, B. Baker, J. Farrell, J. Holt, J. M. Hale, P. Roberson, R. Burlacu, *et al.* (2020). Seismic Analysis of the 2020 Magna, Utah, Earthquake Sequence: Evidence for a Listric Wasatch Fault, *Geophysical Research Letters* **47**, no. 18, e2020GL089798, doi: 10.1029/2020GL089798.

Pang, G., K. D. Koper, M. C. Stickney, J. C. Pechmann, R. Burlacu, K. L. Pankow, S. Payne, and H. M. Benz (2018). Seismicity in the Challis, Idaho, Region, January 2014–May 2017: Late Aftershocks of the 1983 Ms 7.3 Borah Peak Earthquake, *Seismological Research Letters* **89**, no. 4, 1366–1378, doi: 10.1785/0220180058.

Pankow, K. L., M. Stickney, J. Y. Ben-Horin, M. Litherland, S. Payne, K. D. Koper, S. L. Bilek, and K. Bogolub (2019). Regional Seismic Network Monitoring in the Eastern Intermountain West, *Seismological Research Letters* **91**, no. 2A, 631–646, doi: 10.1785/0220190209.

PROJ contributors (2022). PROJ coordinate transformation software library, manual, Open Source Geospatial Foundation, doi: 10.5281/zenodo.5884394.

Ross, Z. E., and E. S. Cochran (2021). Evidence for Latent Crustal Fluid Injection Transients in Southern California From Long-Duration Earthquake Swarms, *Geophysical Research Letters* **48**, no. 12, e2021GL092465, doi: 10.1029/2021GL092465.

Ross, Z. E., E. S. Cochran, D. T. Trugman, and J. D. Smith (2020). 3D fault architecture controls the dynamism of earthquake swarms, *Science* **368**, no. 6497, 1357–1361, doi: 10.1126/science.abb0779.

Ross, Z. E., B. Idini, Z. Jia, O. L. Stephenson, M. Zhong, X. Wang, Z. Zhan, M. Simons, E. J. Fielding, S.-H. Yun, *et al.* (2019). Hierarchical interlocked orthogonal faulting in the 2019 Ridgecrest earthquake sequence, *Science* **366**, no. 6463, 346–351, doi: 10.1126/science.aaz0109.

Ross, Z. E., D. T. Trugman, E. Hauksson, and P. M. Shearer (2019). Searching for hidden earthquakes in Southern California, *Science* **364**, no. 6442, 767–771, doi: 10.1126/science.aaw6888.

Rubinstein, J. L., W. L. Ellsworth, and S. L. Dougherty (2018). The 2013–2016 Induced Earthquakes in Harper and Sumner Counties, Southern Kansas, *Bulletin of the Seismological Society of America* **108**, no. 2, 674–689, doi: 10.1785/0120170209.

Savvaidis, A., S. Hicks, A. Lomax, and M. Shirley (2021). The Importance of Accurate Earthquake Source Information for Understanding the Cause of Induced Seismicity: The Case of Mentone M4.9 Earthquake in West Texas, in *SSA Annual Meeting Abstracts* Annual Meeting: Virtual, 1213–1479, doi: 10.1785/0220210025.

Savvaidis, A., A. Lomax, and C. Breton (2020). Induced Seismicity in the Delaware Basin, West Texas, is Caused by Hydraulic Fracturing and Wastewater Disposal, *Bulletin of the Seismological Society of America* **110**, no. 5, 2225–2241, doi: 10.1785/0120200087.

Savvaidis, A., A. Lomax, R. Dommisse, C. Breton, M. Shirley, and V. O'Sullivan (2022). Induced seismicity hypocentral depth stability and sensitivity to Vp/Vs in the South Delaware Basin, West Texas, in *Second International Meeting for Applied Geoscience & Energy* Houston, Texas, Society of Exploration Geophysicists and American Association of Petroleum Geologists, 1566–1570, doi: 10.1190/image2022-3751081.1.

Savvaidis, A., B. Young, G. D. Huang, and A. Lomax (2019). TexNet: A Statewide Seismological Network in Texas, *Seismological Research Letters* **90**, no. 4, 1702–1715, doi: 10.1785/0220180350.

Shaddox, H. R., and S. Y. Schwartz (2019). Subducted seamount diverts shallow slow slip to the forearc of the northern Hikurangi subduction zone, New Zealand, *Geology* **47**, no. 5, 415–418, doi: 10.1130/G45810.1.

Shearer, P. M. (1997). Improving local earthquake locations using the L1 norm and waveform cross correlation: Application to the Whittier Narrows, California, aftershock sequence, *Journal of Geophysical Research: Solid Earth* **102**, no. B4, 8269–8283, doi: 10.1029/96JB03228.

Shelly, D. R. (2020). A High-Resolution Seismic Catalog for the Initial 2019 Ridgecrest Earthquake Sequence: Foreshocks, Aftershocks, and Faulting Complexity, *Seismological Research Letters* **91**, no. 4, 1971–1978, doi: 10.1785/0220190309.

Sheng, Y., K. S. Pepin, and W. L. Ellsworth (2022). On the Depth of Earthquakes in the Delaware Basin: A Case Study along the Reeves–Pecos County Line, *The Seismic Record* **2**, no. 1, 29–37, doi: 10.1785/0320210048.

Skoumal, R. J., A. J. Barbour, M. R. Brudzinski, T. Langenkamp, and J. O. Kaven (2020). Induced Seismicity in the Delaware Basin, Texas, *Journal of Geophysical Research: Solid Earth* **125**, no. 1, e2019JB018558, doi: 10.1029/2019JB018558.

Skoumal, R. J., J. O. Kaven, and J. I. Walter (2019). Characterizing Seismogenic Fault Structures in Oklahoma Using a Relocated Template-Matched Catalog, *Seismological Research Letters* **90**, no. 4, doi: 10.1785/0220190045.

Skoumal, R. J., and D. T. Trugman (2021). The Proliferation of Induced Seismicity in the Permian Basin, Texas, *Journal of Geophysical Research: Solid Earth* **126**, no. 6, e2021JB021921, doi: 10.1029/2021JB021921.

Staniewicz, S., J. Chen, H. Lee, J. Olson, A. Savvaidis, R. Reedy, C. Breton, E. Rathje, and P. Hennings (2020). InSAR Reveals Complex Surface Deformation Patterns Over an 80,000 km2 Oil-Producing Region in the Permian Basin, *Geophysical Research Letters* **47**, no. 21, e2020GL090151, doi: 10.1029/2020GL090151.

Trugman, D. T. (2020). Stress-Drop and Source Scaling of the 2019 Ridgecrest, California, Earthquake Sequence, *Bulletin of the Seismological Society of America* **110**, no. 4, 1859–1871, doi: 10.1785/0120200009.

Trugman, D. T., S. L. Dougherty, E. S. Cochran, and P. M. Shearer (2017). Source Spectral Properties of Small to Moderate Earthquakes in Southern Kansas, *J. Geophys. Res. Solid Earth* **122**, no. 10, 2017JB014649, doi: 10.1002/2017JB014649.

Trugman, D. T., Z. E. Ross, and P. A. Johnson (2020). Imaging Stress and Faulting Complexity Through Earthquake Waveform Similarity, *Geophysical Research Letters* **47**, no. 1, e2019GL085888, doi: 10.1029/2019GL085888.

Trugman, D. T., and A. Savvaidis (2021). Source Spectral Properties of Earthquakes in the Delaware Basin of West Texas, *Seismological Research Letters* **92**, no. 4, 2477–2489, doi: 10.1785/0220200461.

Trugman, D. T., and P. M. Shearer (2017). GrowClust: A Hierarchical Clustering Algorithm for Relative Earthquake Relocation, with Application to the Spanish Springs and Sheldon, Nevada, Earthquake Sequences, *Seismological Research Letters* **88**, no. 2A, 379–391, doi: 10.1785/0220160188.

Ulrich, T., A.-A. Gabriel, J.-P. Ampuero, and W. Xu (2019). Dynamic viability of the 2016 Mw 7.8 Kaikōura earthquake cascade on weak crustal faults, 1, *Nature Communications* **10**, no. 1, 1213, doi: 10.1038/s41467-019-09125-w.

Waldhauser, F., and W. L. Ellsworth (2000). A Double-Difference Earthquake Location Algorithm: Method and Application to the Northern Hayward Fault, California, *Bulletin of the Seismological Society of America* **90**, no. 6, 1353–1368, doi: 10.1785/0120000006.

Waldhauser, F., and W. L. Ellsworth (2002). Fault structure and mechanics of the Hayward Fault, California, from double-difference earthquake locations, *J. Geophys. Res.* **107**, no. B3, ESE 3-1, doi: 10.1029/2000JB000084.

Waldhauser, F., and D. P. Schaff (2008). Large-scale relocation of two decades of Northern California seismicity using cross-correlation and double-difference methods, *Journal of Geophysical Research* **113**, no. B8, doi: 10.1029/2007JB005479.

Wessel, P., J. F. Luis, L. Uieda, R. Scharroo, F. Wobbe, W. H. F. Smith, and D. Tian (2019). The Generic Mapping Tools Version 6, *Geochemistry, Geophysics, Geosystems* **20**, no. 11, 5556–5564, doi: https://doi.org/10.1029/2019GC008515.

Williams, C. A., D. Eberhart-Phillips, S. Bannister, D. H. N. Barker, S. Henrys, M. Reyners, and R. Sutherland (2013). Revised Interface Geometry for the Hikurangi Subduction Zone, New Zealand, *Seismological Research Letters* **84**, no. 6, 1066–1073, doi: 10.1785/0220130035.

Wolfe, C. J. (2002). On the Mathematics of Using Difference Operators to Relocate Earthquakes, *Bulletin of the Seismological Society of America* **92**, no. 8, 2879–2892, doi: 10.1785/0120010189.

690 Zhai, G., M. Shirzaei, and M. Manga (2021). Widespread deep seismicity in the Delaware Basin, Texas, is mainly
691 driven by shallow wastewater injection, *PNAS* **118**, no. 20, doi: 10.1073/pnas.2102338118.

692 Zhang, H., K. D. Koper, K. Pankow, and Z. Ge (2017). Imaging the 2016 Mw 7.8 Kaikoura, New Zealand,
693 earthquake with teleseismic P waves: A cascading rupture across multiple faults, *Geophysical Research*
694 *Letters* **44**, no. 10, 4790–4798, doi: 10.1002/2017GL073461.

695

696 **Mailing Addresses:**

697 Daniel T. Trugman: Nevada Seismological Laboratory, University of Nevada, Reno. Laxalt

698 Mineral Engineering Building, Room 322, University of Nevada, Reno, Reno NV 89557.

699 Calum J. Chamberlain: School of Geography, Environment and Earth Sciences, Victoria

700 University of Wellington. CO 505, Cotton Building (All Blocks), Gate 7, Kelburn Parade,

701 Wellington, 6012, New Zealand.

702 Alexandros Savvaidis: Bureau of Economic Geology, The University of Texas at Austin.

703 University Station Box X, Austin, TX 78713-8924.

704 Anthony Lomax: ALomax Scientific, 320 Chemin de Indes, 06379 Mouans-Sartoux, France.

Figures

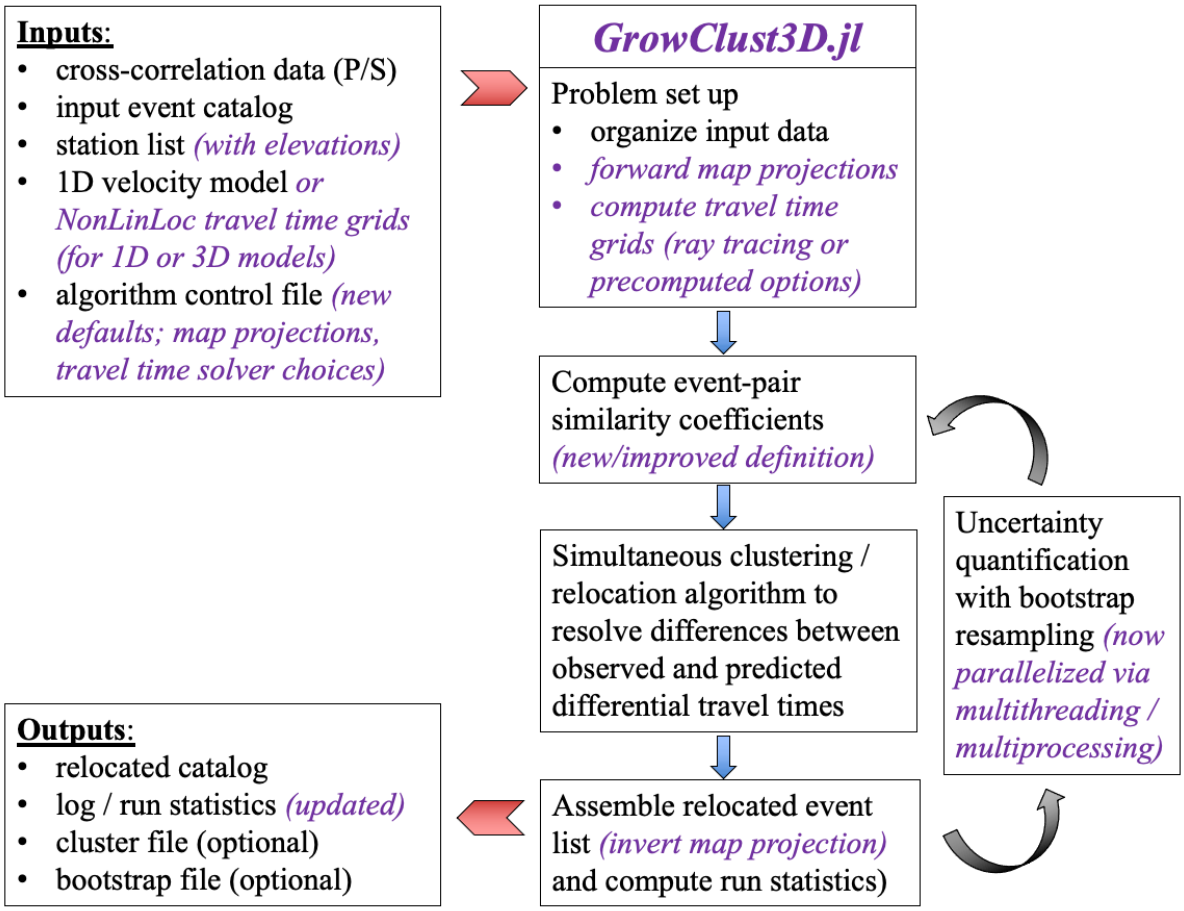

Figure 1. Schematic overview of the GrowClust3D.jl workflow, with newly available features italicized for emphasis.

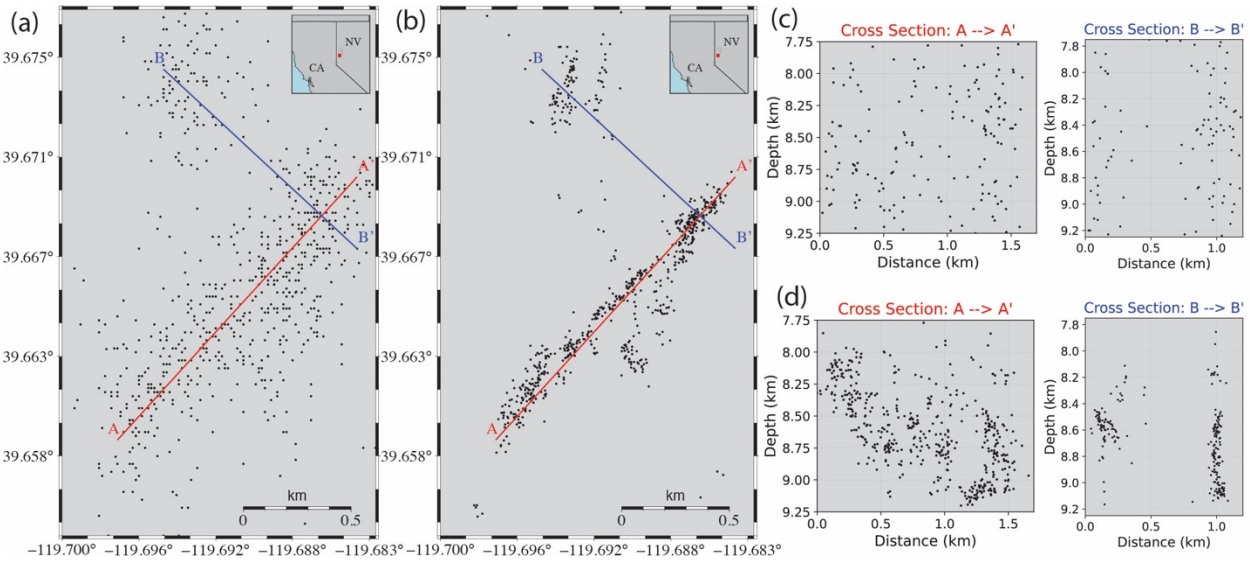

709

710 **Figure 2**. Relocation of the Spanish Springs, Nevada earthquake sequence. Panels (a) and (b)

711 compare the input catalog reported by the Nevada Seismological Laboratory and to the

712 GrowClust3D.jl-relocated relocated catalog in map view. Panels (c) and (d) compare input and

713 relocated catalogs in cross section.

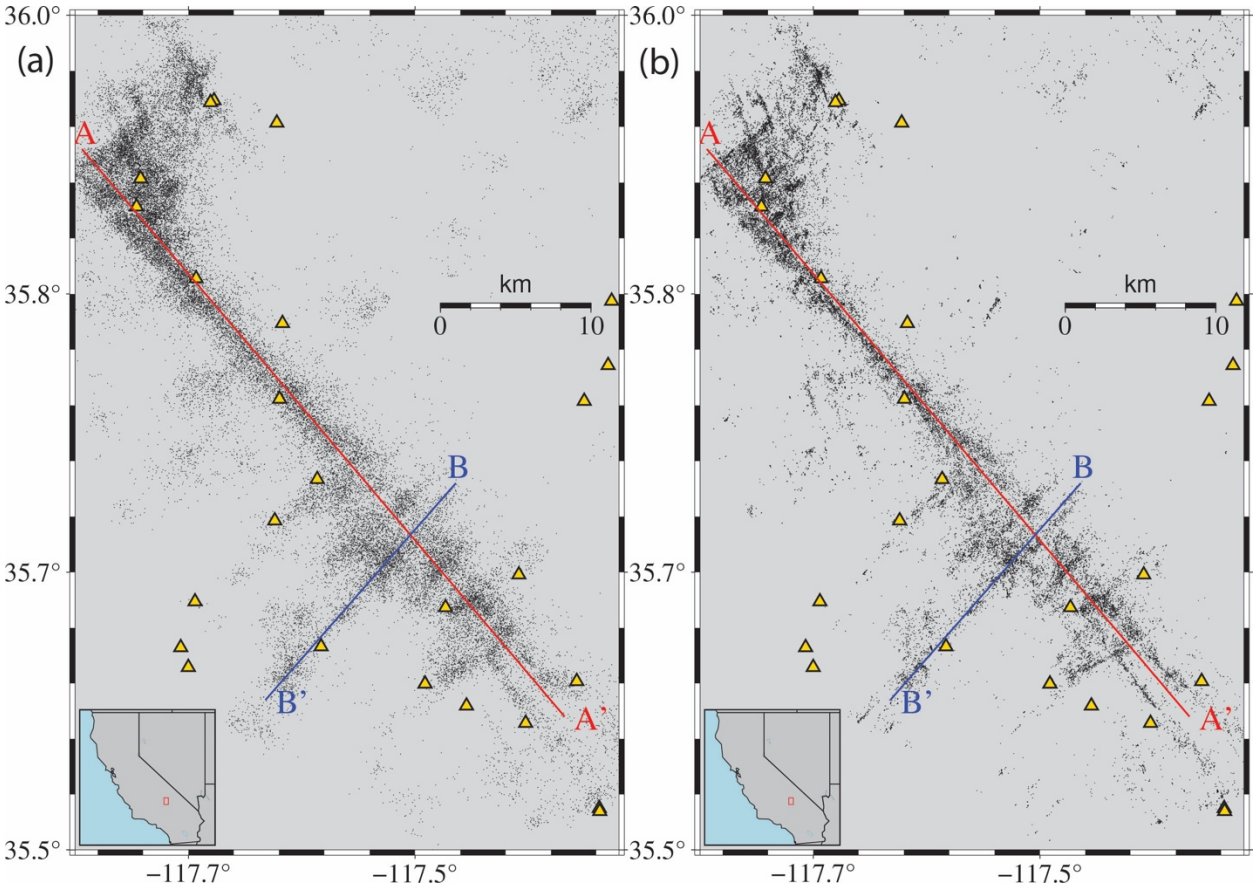

Figure 3. Map view of the Ridgecrest, California sequence comparing (a) the input catalog from the Southern California Earthquake Data Center and (b) the GrowClust3D.jl-relocated catalog. Station locations are marked with triangles. Note the definition of cross sections A-A' and B-B' that are used in Figure 4.

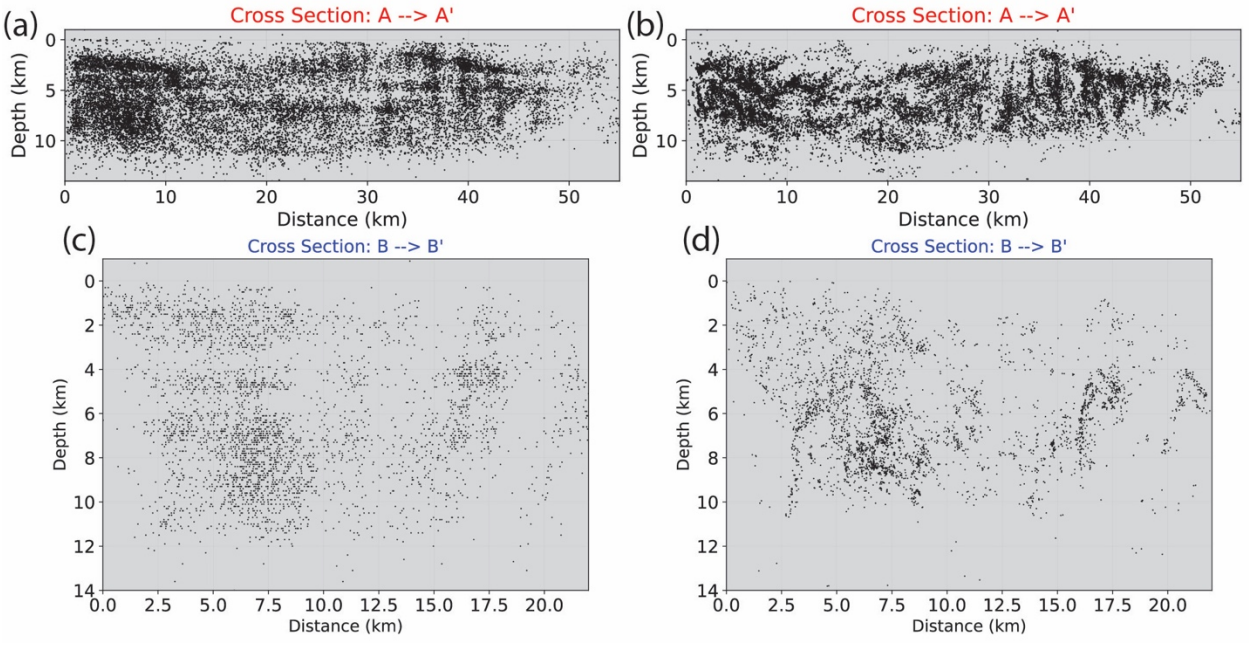

Figure 4. Depth cross-sections for the relocation of the Ridgecrest, California sequence. Panels (a) and (c) show cross-sections of the input catalog from the Southern California Earthquake Data Center, while panels (b) and (d) show cross-sections of GrowClust3D.jl-relocated seismicity. Cross sections A-A' and B-B' are defined in Figure 3.

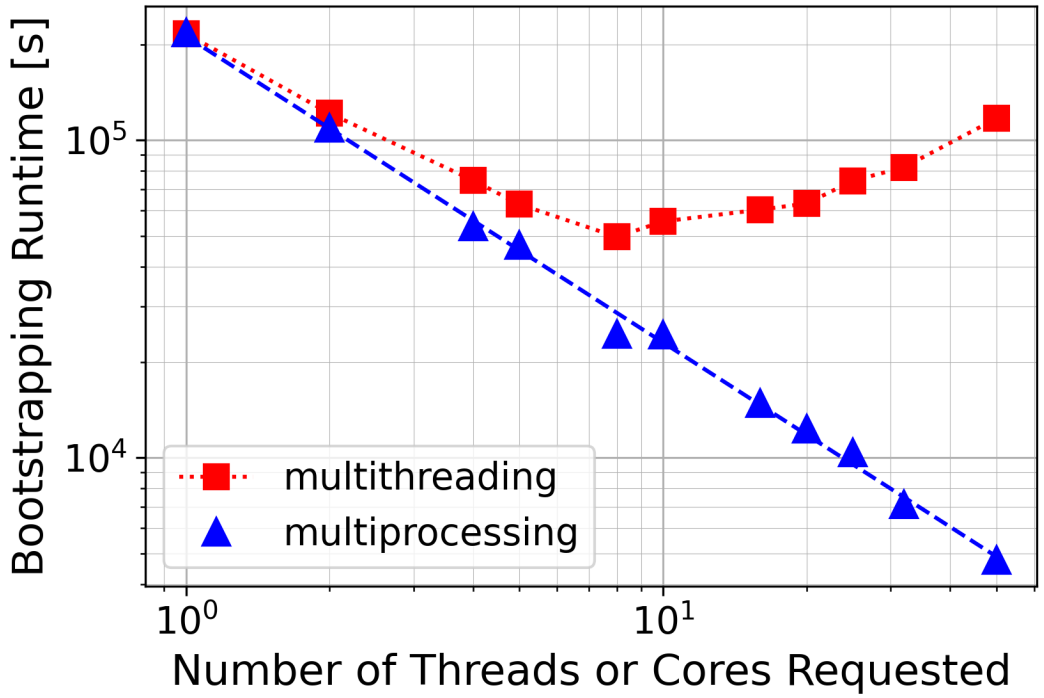

Figure 5. Parallelization experiments. Comparison of multithreading (square symbols) and multiprocessing (triangle symbols) runtime for 100 bootstrap resampling runs of the Ridgecrest sequence. Note log-log scale, where the x-axis refers to the number of threads or cores requested.

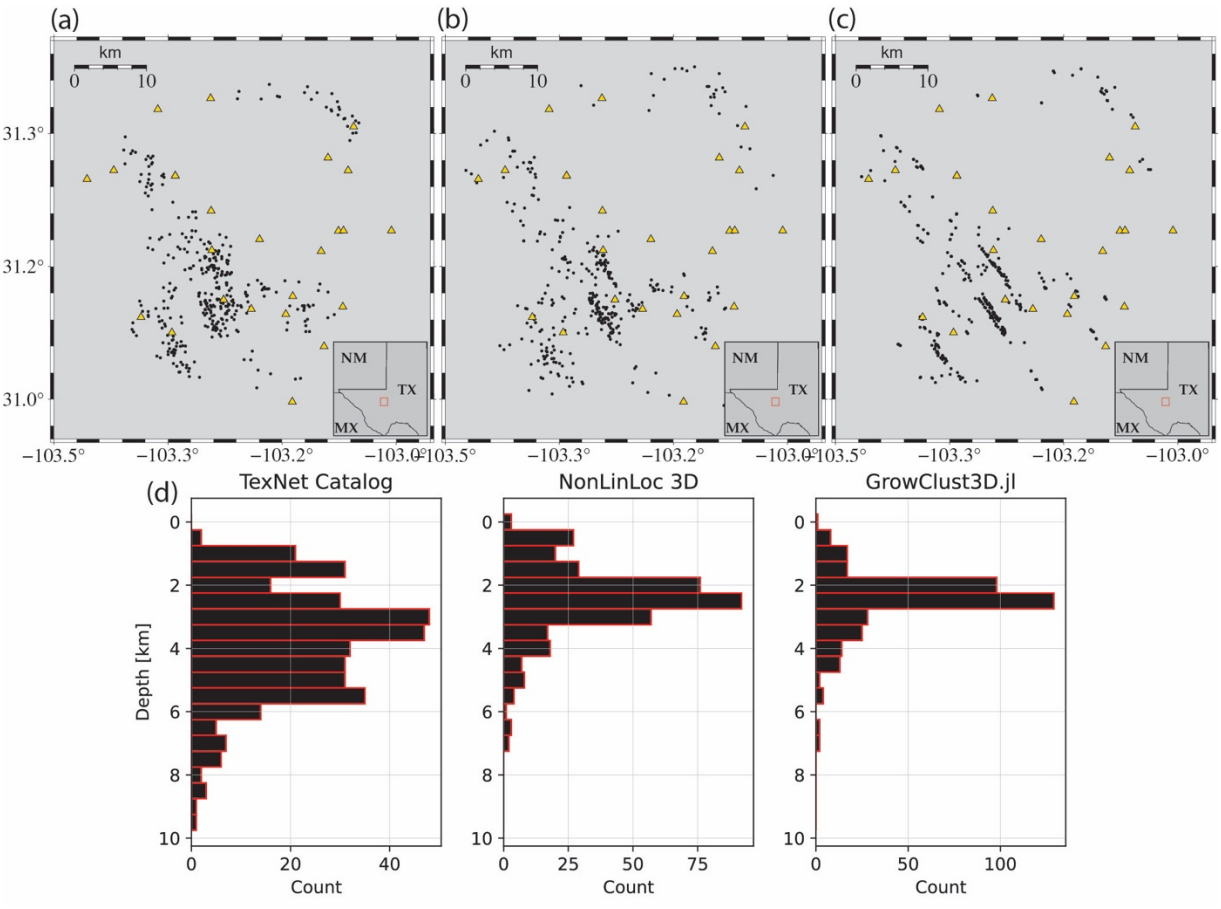

732

733 **Figure 6**. Relocation of seismicity near Coyanosa, Texas (USA). (a) TexNet catalog locations
734 shown in map view. (b) Refined absolute locations of these events using NonLinLoc and a 3D
735 velocity model. (c) Refined relative relocations of these events using GrowClust3D.jl. (d)
736 Comparison of the depth distributions of seismicity for the TexNet catalog (1D model),
737 NonLinLoc (3D model), and GrowClust3D.jl (3D model). In each panel, only the 364 events that
738 are relocated by GrowClust3D.jl are shown. Station locations are marked with triangles for
739 reference in panels (a) through (c).

740

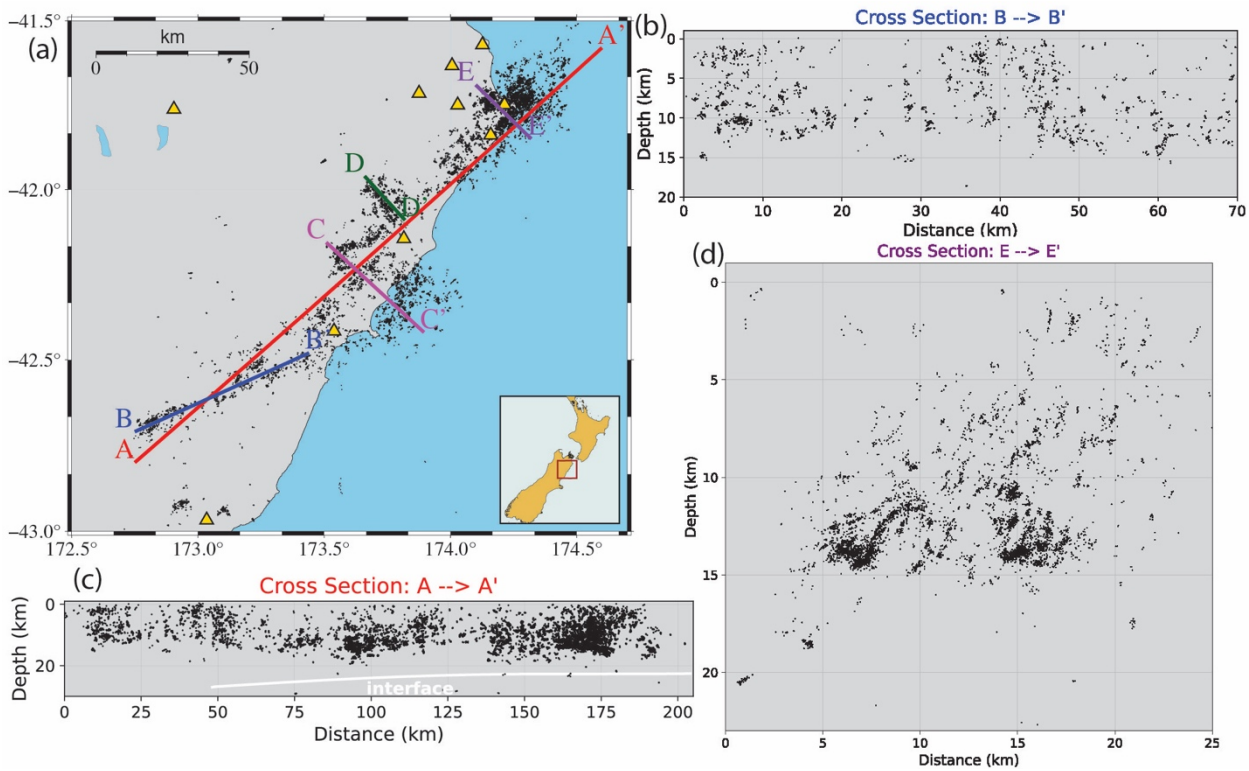

Figure 7. GrowClust3D.jl relocations of the Kaikōura earthquake sequence in map view (panel a) and select cross-sections (panels bcd). Station locations are marked in triangles, with the position of the subduction interface from Williams *et al.* (2013) marked with a solid line.

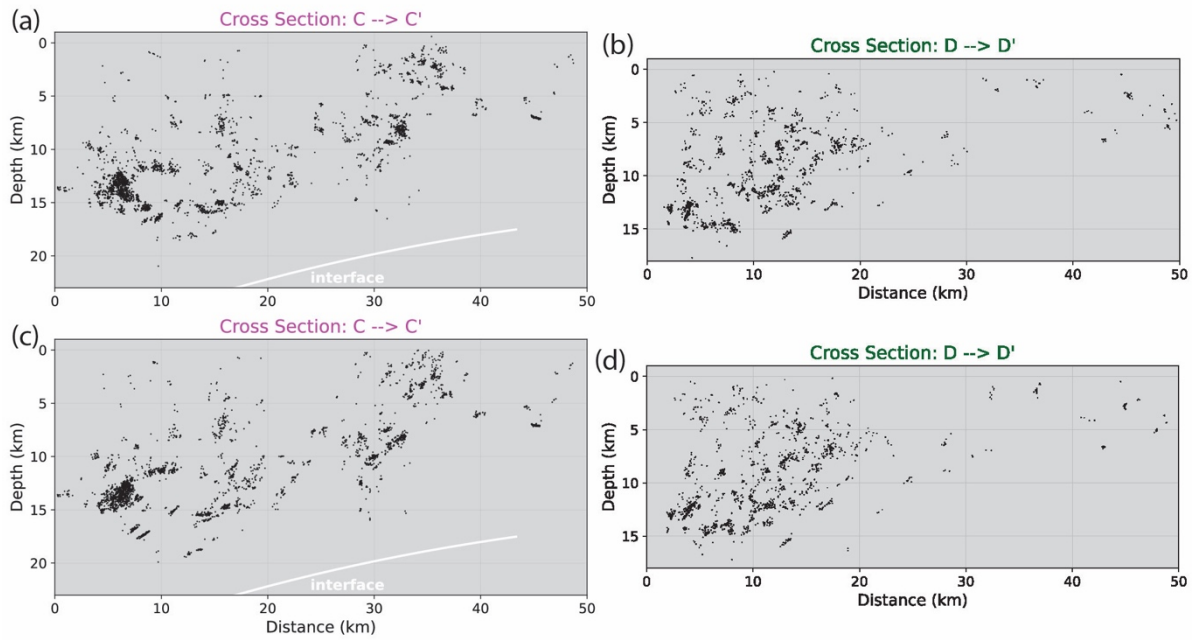

Figure 8. Comparison of the GrowClust relocations of Chamberlain et al. (2021) in panels (a) and (b) with GrowClust3D.jl relocation (this study) in panels (c) and (d). Cross-sections C-C' and D-D' are defined in Figure 7. While both datasets are waveform-relocated, the GrowClust3D.jl solution more clearly resolves the details and dip of possible linear splay faulting structures in cross-section C-C'.